Stem Cell Reports
Article

OPEN ACCESS

Neurite Collapse and Altered ER Ca^{2+} Control in Human Parkinson Disease Patient iPSC-Derived Neurons with LRRK2 G2019S Mutation

Joanna A. Korecka,[1,*] Sebastien Talbot,[2,4] Teresia M. Osborn,[1] Sherida M. de Leeuw,[1] Simon A. Levy,[1] Eliza J. Ferrari,[1] Alyssa Moskites,[1] Elise Atkinson,[1] Francine M. Jodelka,[3] Anthony J. Hinrich,[3] Michelle L. Hastings,[3] Clifford J. Woolf,[2] Penelope J. Hallett,[1] and Ole Isacson[1,*]

[1]Neuroregeneration Research Institute, Harvard Medical School/McLean Hospital, Belmont, MA 02478, USA
[2]F.M. Kirby Neurobiology Center, Boston Children's Hospital, Department of Neurobiology, Harvard Medical School, Boston, MA 02115, USA
[3]Center for Genetics Diseases, Chicago Medical School, Rosalind Franklin University of Medicine and Science, North Chicago, IL 60064, USA
[4]Present address: Département de Pharmacologie et Physiologie, Université de Montréal, Montréal, QC H3T 1J4, Canada
*Correspondence: jkorecka@mclean.harvard.edu (J.A.K.), ole_isacson@hms.harvard.edu (O.I.)
https://doi.org/10.1016/j.stemcr.2018.11.021

SUMMARY

The Parkinson disease (PD) genetic LRRK2 gain-of-function mutations may relate to the ER pathological changes seen in PD patients at postmortem. Human induced pluripotent stem cell (iPSC)-derived neurons with the PD pathogenic LRRK2 G2019S mutation exhibited neurite collapse when challenged with the ER Ca^{2+} influx sarco/ER Ca^{2+}-ATPase inhibitor thapsigargin (THP). Baseline ER Ca^{2+} levels measured with the ER Ca^{2+} indicator CEPIA-ER were lower in LRRK2 G2019S human neurons, including in differentiated midbrain dopamine neurons *in vitro*. After THP challenge, PD patient-derived neurons displayed increased Ca^{2+} influx and decreased intracellular Ca^{2+} buffering upon membrane depolarization. These effects were reversed following LRRK2 mutation correction by antisense oligonucleotides and gene editing. Gene expression analysis in LRRK2 G2019S neurons identified modified levels of key store-operated Ca^{2+} entry regulators, with no alterations in ER Ca^{2+} efflux. These results demonstrate PD gene mutation LRRK2 G2019S ER calcium-dependent pathogenic effects in human neurons.

INTRODUCTION

The leucine-rich repeat kinase 2 (LRRK2) G2019S gain-of-function mutation, which increases LRRK2 kinase activity (Islam and Moore, 2017; West et al., 2005), is one of the most prevalent autosomal dominant mutations contributing to Parkinson disease (PD) pathogenesis with variable penetrance. Genetic variations in the LRRK2 locus are also associated with an increased risk for sporadic PD development (Nalls et al., 2014). The G2019S-dependent increase in kinase activity is implicated in organelle mechanisms such as mitochondrial function, transport, and mobility (Cooper et al., 2012; Sanders et al., 2014; Smith et al., 2016); neurite outgrowth (Reinhardt et al., 2013; Sanchez-Danes et al., 2012); endosomal and vesicle transport (Rivero-Rios et al., 2015; Steger et al., 2016); autophagy (Schapansky et al., 2014) and Ca^{2+}-dependent autophagosome formation (Gomez-Suaga et al., 2012); mitophagy (Hsieh et al., 2016); and calcium homeostasis (Bedford et al., 2016; Cherra et al., 2013; Schwab and Ebert, 2015; Verma et al., 2017; Yan et al., 2015). However, the molecular mechanisms that link these multiple cellular functions with the LRRK2 G2019S mutation are not well understood.

Calcium signaling controls cellular processes such as exocytosis, synaptic plasticity, gene transcription, oxidative phosphorylation, and organelle function (Sano and Reed, 2013). Alterations in the intracellular Ca^{2+} homeostasis are linked to neurodegeneration in PD (Guzman et al., 2010; Hurley et al., 2013). The ER lumen is a major intracellular Ca^{2+} storage facility (Lam and Galione, 2013), with Ca^{2+}-binding chaperones mediating protein folding. Given that the ER network extends throughout the cell and forms junctions with other cellular organelles such as mitochondria, plasma membrane, and lysosomes, which is crucial for coordinating and integrating intracellular Ca^{2+} signals necessary for organelle communication and function (Lam and Galione, 2013; Wu et al., 2017), we investigated how LRRK2 G2019S mutations associated with PD influence ER calcium control. Importantly, ER Ca^{2+} fluctuations may have an impact on protein-folding capacity and contribute to ER stress (Sano and Reed, 2013). Increased expression of ER stress markers is found in postmortem human PD brain tissue (Hoozemans et al., 2007), and based on a meta-analysis of multiple genome-wide association studies, the ER stress response appears to be a contributor to the development of PD pathology (Klemann et al., 2017).

To understand the role of ER calcium regulation in LRRK2-dependent cellular function, we used PD patient stem cell-derived neurons to examine intracellular and ER-specific calcium homeostasis and effects of ER calcium inhibition on neuronal function. Employing both LRRK2-targeted gene correction and antisense oligonucleotide (ASO) technology, we set out to determine the direct role of LRRK2 protein function in ER calcium control.

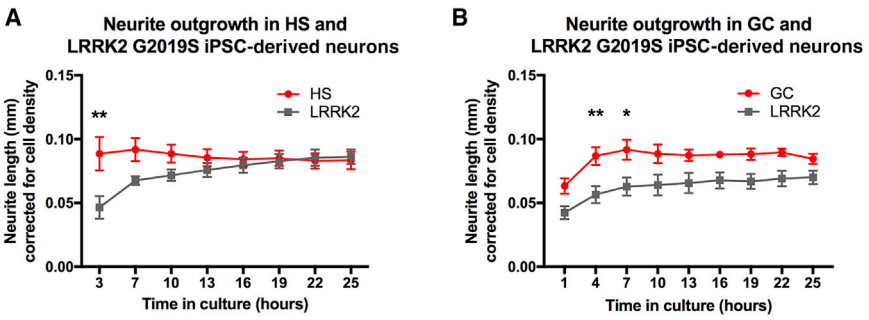

Figure 1. Neurite Outgrowth Is Initially Decreased in Human iPSC-Derived Neurons Carrying the LRRK2 G2019S Mutation

(A) Shortly after plating, the speed of neurite outgrowth is significantly decreased in the human iPSC-derived neurons carrying the LRRK2 G2019S mutation (LRRK2; N = 3 independent PD patient lines: 29F, 9A, PD28 clone 1) compared with the healthy subject (HS; N = 3 independent HS lines 10A, 21.31, and 21.35) control neurons ($p = 0.0018$, $F_{(1,32)} = 11.55$).

(B) Similarly, when using a new cohort of PD patient iPSC-derived neurons, neurite outgrowth is initially decreased in LRRK2 neurons (N = 4 [N = 2 independent PD patient lines with 2 clones per line: IM1Mut -L2-1Mut, IM2Mut-L2-2Mut, T4.6(Mut)-L1-1Mut, T4.13(Mut)-L1-2Mut, see Table S1]) compared with their gene-corrected (GC) isogenic controls ($p < 0.0001$, $F_{(1,36)} = 62.76$, N = 4 [N = 2 independent GC lines with 2 clones per line: IM1GC-L2-1GC, IM2GC-L2-2GC, T4.6.43(GC)-L1-1GC2, T4.13.10(GC)-L1-2GC, see Table S1]). Within 24 hr these outgrowth differences are no longer observed, as the neurites stabilize their networks. Each cell line represents a pool of 3 wells as technical replicates.

Statistical analysis was performed using two-way ANOVA with Sidak's multiple testing correction (MTC). *$p < 0.05$, **$p < 0.01$. Error bars represent SEM.

RESULTS

Inhibition of ER Ca^{2+} Influx Induces Neurite Collapse in PD Patient iPSC-Derived LRRK2 G2019S Neurons

Given that ER stress plays a role in PD pathology (Hoozemans et al., 2007; Klemann et al., 2017), with ER Ca^{2+} fluctuations influencing the protein folding capacity of ER chaperones and contributing to ER stress (Sano and Reed, 2013), we decided to determine if ER inhibition of Ca^{2+} influx by thapsigargin (THP) would have a differential effect on neuronal vulnerability in established long-term human neuronal cultures derived from PD patients carrying the LRRK2 G2019S mutation. Upon the induction of ER stress with THP, the LRRK2 G2019S mutation did not change the expression regulation of the key ER stress response genes or the *XBP1* splicing (Figure S1).

The LRRK2 G2019S mutation decreased the speed of axonal outgrowth *in vitro* in PD patient induced pluripotent stem cell (iPSC)-derived neurons shortly after plating (Figure 1), confirming the basic observation of decreased neurite length in previous reports (Reinhardt et al., 2013). Furthermore, live cell imaging showed that neurite length stabilized over time in culture.

To study the role of ER Ca^{2+} on neurite outgrowth, sarco/ER Ca^{2+}-ATPase (Serca) inhibition was performed by THP treatment on the iPSC-derived neurons at 1 week of culture. Neurite length was significantly decreased in LRRK2 G2019S iPSC-derived neurons treated with 10 and 100 nM THP (Figure 2A, 10 nM, $p = 0.0214$, $F_{(1.01,\ 2.04)} = 43.27$; 100 nM, $p = 0.035$, $F_{(1.13,\ 2.26)} = 21.1$). This effect was not observed in healthy subject (HS) control iPSC-derived neurons (Figure 2B, 10 nM, $p = 0.0586$, $F_{(1,2)} = 15.58$; 100 nM, $p = 0.1183$, $F_{(1,\ 2)} = 6.969$) and, when replicated in an independent experiment, it was rescued by LRRK2 exon 41-specific ASO application (Figure 2C, 10 nM, $p = 0.0175$, $F_{(2,\ 6)} = 8.563$; 100 nM, $p = 0.0063$, $F_{(2,\ 6)} = 13.26$; and Figure 2D, 10 nM, $p = 0.1582$, $F_{(2,\ 6)} = 2.546$; 100 nM, $p = 0.6274$, $F_{(2,\ 6)} = 0.5043$; only ASO-transfected (ASO+) cells selected for analysis), designed to instigate LRRK2 pre-mRNA exon 41 skipping containing the G2019S mutation. Exon 41 ASO treatment induced ~60% of exon 41 skipping (Figures S2A and S2B) and reduced the LRRK2 protein level by 27% (Figure S2C). ASO transfection efficiency varied from 30% to 90% between experiments and between different neuronal iPSC-derived lines. Ex41 ASO had no effect on the neurite outgrowth in the HS iPSC-derived neurons (Figures S3A and S3B). The SERCA inhibition-dependent axonal collapse was further confirmed in an additional independent set of PD patient iPSC-derived neurons carrying the G2019S mutation (Figure 2E, 10 nM, $p = 0.0004$, $F_{(1.02,\ 3.08)} = 297$; 100 nM, $p = 0.0002$, $F_{(1.50,\ 4.52)} = 106.1$), and rescued by isogenic gene correction of the G2019S mutation by gene editing (Figure 2F, 10 nM, $p = 0.2665$, $F_{(1.29,\ 3.86)} = 1.785$; 100 nM, $p = 0.088$, $F_{(1.20,\ 3.60)} = 5.341$). Finally, LRRK2 G2019S neurons were exposed to LRRK2 kinase inhibitor MLi-2 (Fell et al., 2015), which consequently rescued neurite collapse induced by low-dose 10 nM THP treatment (Figure 2G, vehicle, $p = 0.0417$, F statistic 6.5; 10 nM MLi-2, $p = 0.1776$, $F_{(2,\ 6)} = 2.337$; 100 nM MLi-2, $p = 0.4306$, Friedman statistic 2). A lower THP concentration (1 nM) or vehicle treatment (EtOH) did not induce any changes

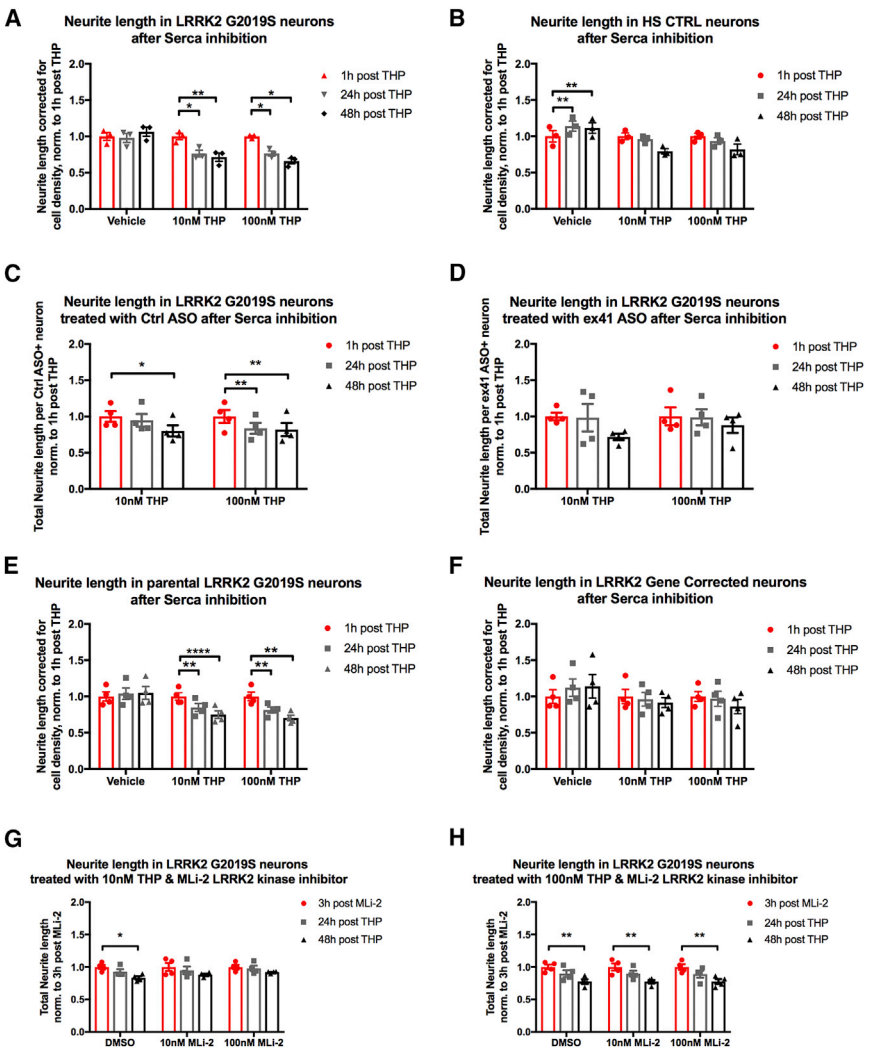

Figure 2. ER Ca^{2+} Influx Reduction through Serca Inhibition Induces Neurite Collapse in PD Patient iPSC-Derived LRRK2 G2019S Neurons

(A) ER Ca^{2+} pump Serca inhibition induced by 10 nM ($p = 0.0214$, $F_{(1.02,\ 2.04)} = 43.27$) and 100 nM ($p = 0.035$, $F_{(1.13,\ 2.26)} = 21.1$) thapsigargin (THP) treatment prompts neurite collapse in LRRK2 G2019S neurons (N = 3 independent PD patient lines 29F, 9A, PD28 clone 1) already at 24 hr post THP treatment.

(B) HS control neurons (N = 3 independent HS lines: 10A, 21.31, and 21.35) do not show neurite collapse after THP treatment (10 nM, $p = 0.0586$, $F_{(1,\ 2)} = 15.58$; 100 nM, $p = 0.1183$, $F_{(1,\ 2)} = 6.969$). We observed an increase in neurite length in the HS neurons when treated with vehicle ($p = 0.0022$, $F_{(1.13,\ 2.27)} = 257.4$). The y axis represents neurite length corrected for cell cluster, normalized to the values of 1 hr post THP per treatment condition.

(C) In an independent differentiation, neurite collapse was confirmed in control ASO (Ctrl ASO)-treated PD patient LRRK2 neurons (N = 4 [N = 3 independent PD patient lines with 1 line containing 2 clones: 29F, 9A, PD28 clone 1, and PD28 clone 2]) upon 10 nM ($p = 0.0175$, $F_{(2,6)} = 8.563$) and 100 nM ($p = 0.0063$, $F_{(2,\ 6)} = 13.26$) THP treatment.

(D) Transfection of the LRRK2 neurons (N = 4 [N = 3 independent PD patient lines with 1 line containing 2 clones: 29F, 9A, PD28 clone 1, and PD28 clone 2]) with the exon 41 ASO (ex41 ASO), inducing exon 41 skipping (see Figures S2B and S2C), rescued the SERCA inhibition-induced neurite collapse in these cells (10 nM, $p = 0.1582$, $F_{(2,\ 6)} = 2.546$; 100 nM, $p = 0.6274$, $F_{(2,\ 6)} = 0.5043$). The y axis represents total ASO-carboxyfluorescein-positive (ASO+) neurite length per ASO+ neuronal count, normalized to 1 hr post THP per treatment condition.

(E) An independent set of PD patient lines (N = 4 [N = 2 independent PD patient lines with 2 clones per line: IM1Mut -L2-1Mut, IM2Mut-L2-2Mut, T4.6(Mut)-L1-1Mut, T4.13(Mut)-L1-2Mut, see Table 1]) also showed neurite collapse after THP-induced Serca inhibition (10 nM, $p = 0.0004$, $F_{(1.02,\ 3.08)} = 297$; 100 nM, $p = 0.0002$, $F_{(1.50,4.52)} = 106.1$). Only ASO+ cells were used for the analysis.

(F) The isogenic GC control neurons, pairs to LRRK2 neurons from (E) (Reinhardt et al., 2013) (N = 4 [N = 2 independent GC lines with 2 clones per line: IM1GC-L2-1GC, IM2GC-L2-2GC, T4.6.43(GC)-L1-1GC2, T4.13.10(GC)-L1-2GC, see Table S1]), do not show neurite collapse after THP treatment (10 nM, $p = 0.2665$, $F_{(1.29,\ 3.86)} = 1.785$; 100 nM, $p = 0.0880$, $F_{(1.20,\ 3.60)} = 5.341$).

(G) In an independent experiment, LRRK2 kinase inhibitor MLi-2 rescued neurite collapse induced by 10 nM THP treatment in LRRK2 neurons (DMSO, $p = 0.0417$, Friedman statistic 6.5; 10 nM MLi-2, $p = 0.1776$, $F_{(2,\ 6)} = 2.337$; 100 nM MLi-2, $p = 0.4306$, Friedman statistic 2).

(H) MLi-2 kinase inhibition does not affect neurite collapse after a high-dose 100 nM THP treatment (DMSO, $p = 0.0052$, $F_{(2,\ 6)} = 14.29$; 10 nM MLi-2, $p = 0.0081$, $F_{(2,\ 6)} = 11.91$; 100 nM MLi-2, $p = 0.0096$, $F_{(2,\ 6)} = 11.13$). For (G) and (H) the same set of PD patient lines was used as in (E) (N = 4 [N = 2 independent PD patient lines with 2 clones per line, IM1Mut -L2-1Mut, IM2Mut-L2-2Mut, T4.6(Mut)-L1-1Mut, T4.13(Mut)-L1-2Mut]). Each cell line represents a pool of 3 wells as technical replicates.

Statistical analysis was performed using repeated-measure one-way ANOVA with Dunnett's MTC or Friedman test with Dunn's MTC, where values were compared with the 1 hr post THP time point or 3 hr post MLi-2 treatment. *$p < 0.05$, **$p < 0.01$, ****$p < 0.0001$. Error bars represent SEM. See also Figures S2 and S3.

in neurite length in these cultures (data not shown). This result shows that inhibition of ER Ca^{2+} influx results in an increased neuronal vulnerability of LRRK2 G2019S neurons as demonstrated by neurite collapse.

Calcium Homeostasis Is Altered in iPSC-Derived Human Neurons Carrying the LRRK2 G2019S Mutation after Serca Inhibition

Inhibition of ER Ca^{2+} influx induced neurite collapse in human iPSC neurons carrying the LRRK2 G2019S mutation (Figure 2). To determine the dynamics of intracellular Ca^{2+} uptake and buffering in PD patient human iPSC-derived neurons, intracellular Ca^{2+} imaging was performed using live single-cell fura-2-acetoxymethyl ester (fura-2 AM) Ca^{2+} imaging analysis. After 24 hr of THP-induced Serca inhibition (at 10 nM), human iPSC-derived neurons carrying the LRRK2 G2019S mutation exhibited an increase in KCl depolarization-induced Ca^{2+} influx, compared with HS control neurons ($p = 0.0448$, $t = 2.661$, $df = 5$) (Figure 3A). Unbound intracellular Ca^{2+} levels were significantly increased upon prolonged KCl membrane depolarization ($p = 0.0303$, $t = 2.993$, $df = 5$), indicating a decreased cellular capacity for intracellular Ca^{2+} buffering in LRRK2 G2019S neurons (Figure 3A). This phenotype was diminished by treatment of LRRK2 neurons with an ASO targeting the LRRK2 exon 41 sequence (ex41 ASO, Figure 3B, second KCl stimulation, $p = 0.458$, $t = 0.8039$, $df = 5$, and the unbound Ca^{2+} levels, $p = 0.2878$, $t = 1.189$, $df = 5$; only ASO+ cells selected for analysis). Ex41 ASO increased intracellular Ca^{2+} levels ($p = 0.0158$, $t = 7.851$, $df = 2$) and decreased Ca^{2+} buffering ($p = 0.0246$, $t = 6.261$, $df = 2$) in the HS iPSC-derived neurons when treated with THP (Figures S3C–S3F). Ca^{2+} levels were equal in HS and LRRK2 G2019S neurons upon Serca inhibition when treated with ex41 ASO. Interestingly, no differences were observed in Ca^{2+} uptake or Ca^{2+} buffering between vehicle-treated HS and LRRK2 G2019S neurons (Figure 3C, $p = 0.7611$, $t = 0.3212$, $df = 5$ and $p = 0.4813$, $t = 0.7605$, $df = 5$, respectively). These results show that LRRK2 mutation can modulate neuronal ER calcium homeostasis.

ER Ca^{2+} Levels and Gene Expression of Key ER Ca^{2+} Regulators Are Decreased in Human iPSC-Derived Neurons Carrying the LRRK2 G2019S Mutation

To determine how LRRK2 contributes to ER calcium homeostasis, we first performed an ER-specific Ca^{2+} level analysis in LRRK2 G2019S iPSC-derived neurons using an ER-specific Ca^{2+}-measuring organelle-entrapped protein indicator, CEPIA1-ER GFP (Suzuki et al., 2014). The specificity of the ER Ca^{2+} detection was confirmed by a decrease in GFP levels in CEPIA-overexpressing neurons following Serca ER Ca^{2+} influx inhibition with THP (Figure S4). PD patient iPSC-derived LRRK2 G2019S neurons showed lower ER Ca^{2+} levels compared with the HS control iPSC neurons, based on the total CEPIA1-ER GFP intensity (Figure 4A, $p = 0.0349$, $t = 2.871$, $df = 5$). This phenotype was confirmed in an independent experiment with additional HS and PD iPSC lines, where the iPSC-derived neurons were transfected with the non-target Ctrl ASO (Figure 4B, $p = 0.0425$, $F_{(2,\ 12)} = 4.155$). The ER Ca^{2+} deficiency was rescued by treating the PD patient neurons carrying the G2019S mutation with LRRK2 exon 41-specific ASO (Figure 4B, $p = 0.0425$, $F_{(2,\ 12)} = 4.155$, only ASO+ cells selected for analysis). A reduction in baseline ER Ca^{2+} was also observed in midbrain dopamine (DA) iPSC-derived neurons carrying the LRRK2 G2019S mutation (Figure 4C, $p < 0.0001$, K-W statistic 57.32), with ER Ca^{2+} levels increased by treatment with LRRK2 ex41 ASO (Figure 4C, only ASO+ cells selected for analysis). See Figure S2D for ex41 ASO treatment-induced effects in midbrain DA neurons. Ex41 ASO treatment showed a non-significant trend to decrease ER Ca^{2+} levels in the HS iPSC-derived neurons (Figures S3G and S3H).

Next, mRNA transcript expression levels of key molecules regulating ER Ca^{2+} uptake, maintenance, and release were measured in iPSC-derived neurons carrying the LRRK2 G2019S mutation and compared with their isogenic gene-corrected controls (Table 1). We found a significant 46% decrease in the expression of the ER Ca^{2+} sensor *STIM1* ($p = 0.005$, $t = 4.316$, $df = 6$), a 40% decrease in membrane receptor *TRPC1* ($p = 0.0209$, $t = 3.107$, $df = 6$), and a 23% decrease in the Ca^{2+} release-activated Ca^{2+} membrane channel *ORAI1* ($p = 0.0038$, $t = 4.571$, $df = 6$) in the LRRK2 G2019S iPSC neurons compared with their isogenic controls. These three molecules are critical for cellular store-operated Ca^{2+} entry (SOCE). No significant changes were found in the expression of Serca isoforms 2 and 3 (*SERCA2*, $p = 0.0875$, $t = 2.04$, $df = 6$; *SERCA3*, $p = 0.6254$, $t = 0.5144$, $df = 6$), both known to be expressed in the brain (Wu et al., 1995). In addition, there were no significant differences observed in the expression of ER Ca^{2+} efflux ITP receptors (*ITPR*) 1 and 3, or of ryanodine receptors (*RYR*) 2 and 3 (Table 1), in line with the observed equal kinetics of Ca^{2+}-induced Ca^{2+} release (CICR) in the LRRK2 G2019S neurons at baseline or after THP-induced Serca inhibition, measured utilizing the CEPIA-ER GFP biosensor (Figures 4D and 4E).

Finally, a recent study identified Ca^{2+}/calmodulin-dependent protein kinase type 1D (*CamK1D*), a Ca^{2+} influx-activated signaling molecule, as a candidate interactor with the LRRK2 protein (Beilina et al., 2014). *CamK1D* expression levels were found to be 69% decreased in iPSC-derived neurons carrying the LRRK2 G2019S mutation (Table 1, $p = 0.0150$, $t = 3.373$, $df = 6$).

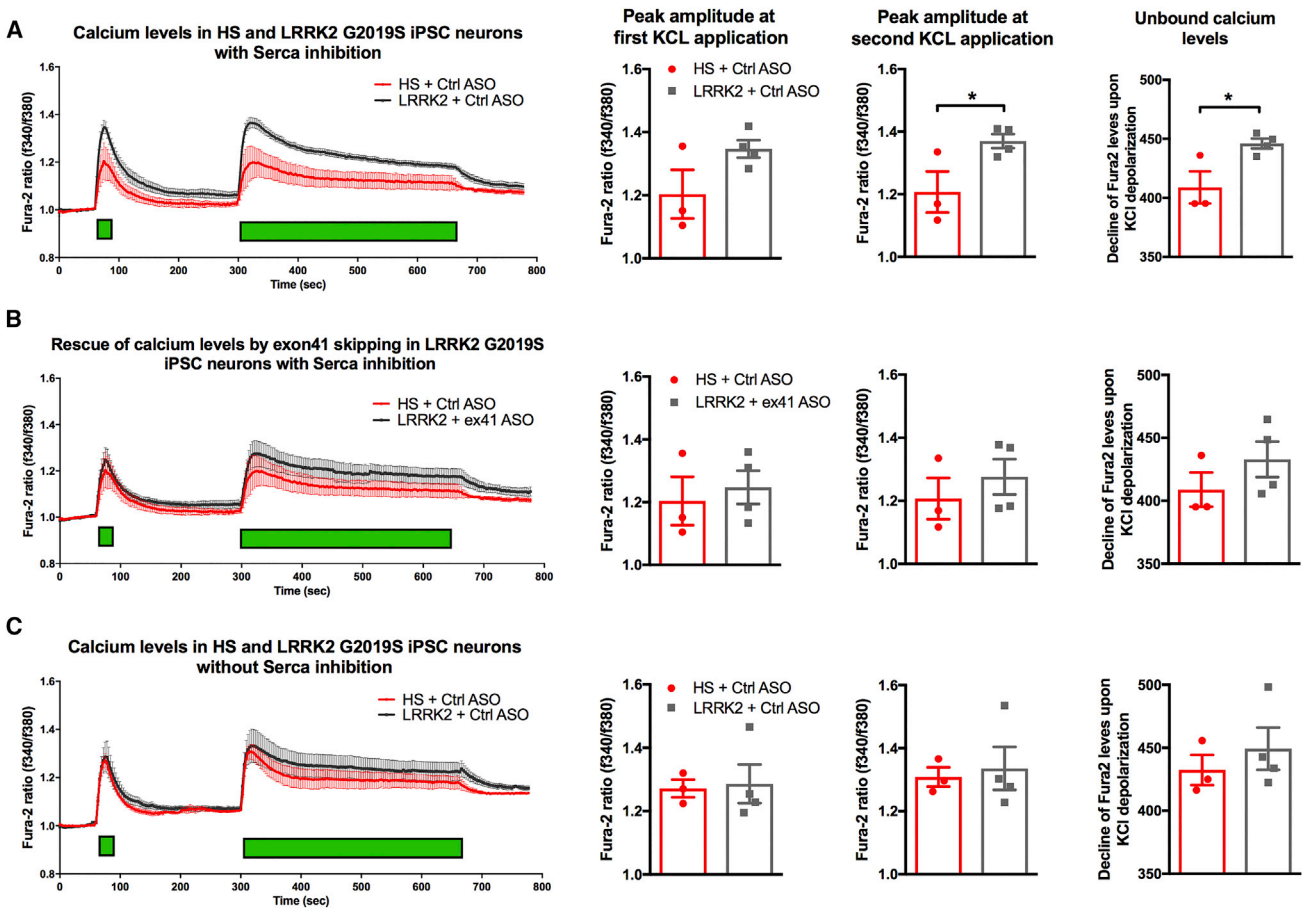

Figure 3. iPSC-Derived Neurons Carrying the LRRK2 G2019S Mutation Show Increased Uptake and Less Buffering of Ca^{2+} after ER Ca^{2+} Pump Serca Inhibition, which Can Be Rescued by LRRK2 Exon 41 Antisense Oligonucleotide

Intracellular Ca^{2+} levels were measured upon KCl stimulation (green bars) in human iPSC-derived neurons using fura-2 AM ratiometric image acquisition.

(A) Upon Serca inhibition with 10 nM THP, intracellular Ca^{2+} levels were significantly increased in LRRK2 neurons (N = 4 [N = 3 independent PD patient lines with 1 line containing 2 clones: 29F, 9A, PD28 clone 1 and PD28 clone 2]) compared with HS (N = 3 independent HS lines: 10A, 21.31, and 21.35) controls. Detailed analysis showed an increase in the second Ca^{2+} peak amplitude upon KCl depolarization ($p = 0.0448$, $t = 2.661$, $df = 5$) and an increase in the unbound Ca^{2+} levels indicating decreased intracellular Ca^{2+} buffering in LRRK2 neurons ($p = 0.0303$ $t = 2.993$, $df = 5$, extrapolated from the area under the fura-2 AM curve during prolonged KCl membrane depolarization).

(B) Neuronal transfection with the LRRK2 exon 41 targeting antisense oligonucleotide (ex41 ASO, see Figures S2B and S2C) normalizes the intracellular Ca^{2+} levels in Serca-blocked iPSC-derived neurons carrying the LRRK2 G2019S mutation (N = 4 [N = 3 independent PD patient lines with 1 line containing 2 clones: 29F, 9A, PD28 clone 1, and PD28 clone 2]). Both the Ca^{2+} amplitude during the second KCl stimulation ($p = 0.458$, $t = 0.8039$, $df = 5$) and the unbound Ca^{2+} levels ($p = 0.2878$, $t = 1.189$, $df = 5$) show equal levels compared with the HS control neurons treated with Ctrl ASO (N = 3 independent healthy subject lines).

(C) Intracellular Ca^{2+} levels were not altered in vehicle-treated LRRK2 neurons (N = 4 [N = 3 independent PD patient lines with 1 line containing 2 clones: 29F, 9A, PD28 clone 1, and PD28 clone 2]) compared with HS controls (N = 3 independent HS lines: 10A, 21.31, and 21.35). Detailed analysis showed no differences in the first ($p = 0.8574$, $t = 0.1892$, $df = 5$) and the second ($p = 0.7611$, $t = 0.3212$, $df = 5$) Ca^{2+} peak amplitude upon KCl depolarization. In addition, there was no difference in Ca^{2+} buffering during the prolonged KCl depolarization ($p = 0.4813$, $t = 0.7605$, $df = 5$), indicating no difference in the binding and compartmentalization of the unbound Ca^{2+}. Each cell line represents a pool of 3 technical replicates resulting in an average of ~90 cells quantified per subject line per treatment condition. Only ASO-carboxyfluorescein-positive cells were used for the analysis.

Statistical analysis was performed using two-tailed unpaired Student's t test. *$p < 0.05$. Error bars represent SEM. See also Figures S2 and S3.

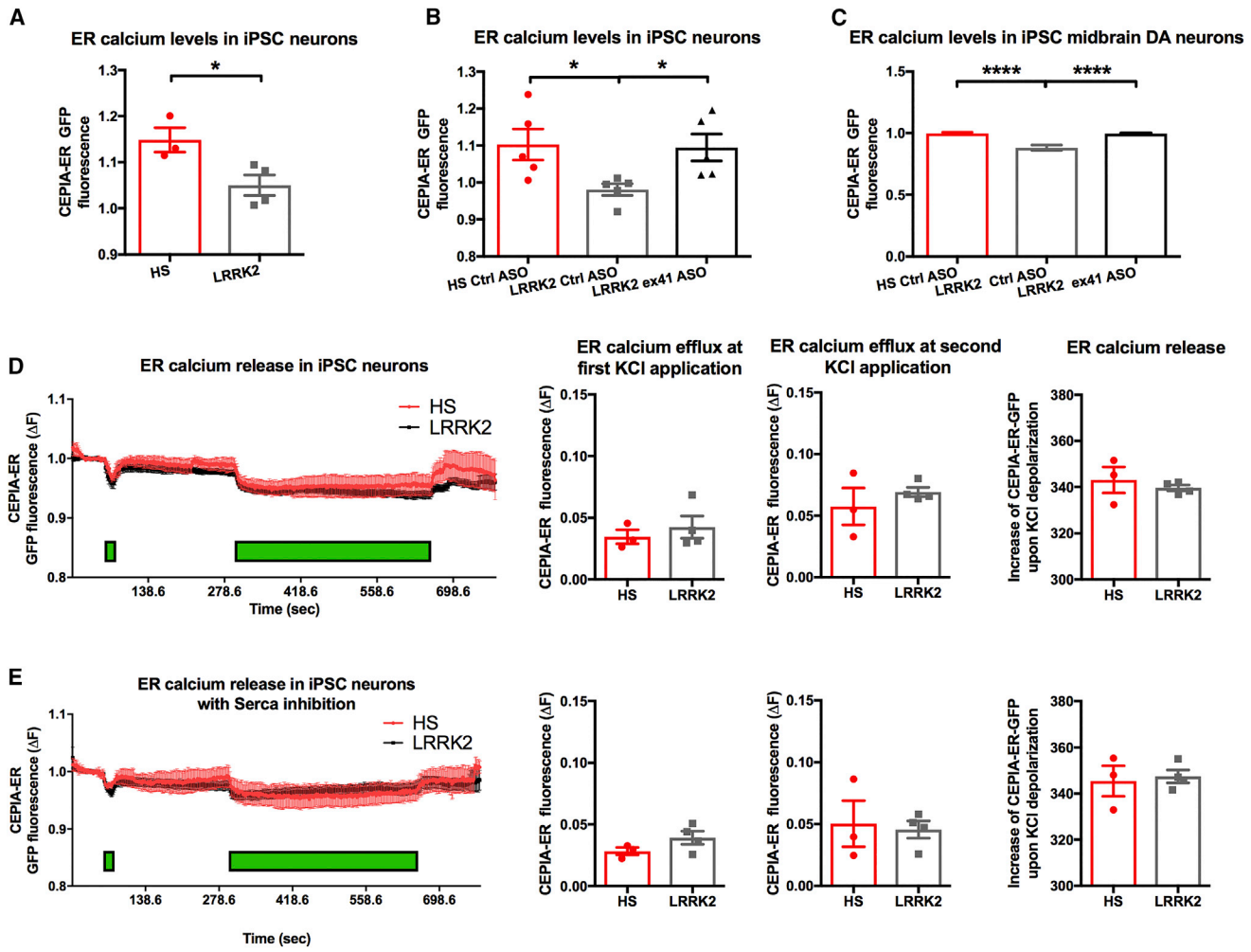

Figure 4. iPSC-Derived Neurons Carrying the LRRK2 G2019S Mutation Show Decreased ER Ca^{2+} Levels

(A) ER Ca^{2+} levels, measured by GFP intensity of CEPIA-ER GFP biosensor probe, were significantly decreased in the mixed-population iPSC neurons carrying the LRRK2 G2019S mutation ($p = 0.0349$, $t = 2.871$, $df = 5$, $N = 4$ [$N = 3$ independent PD patient lines with 1 line containing 2 clones: 29F, 9A, PD28 clone 1 (C1), and PD28 clone 2 (C2)]) compared with HS control neurons ($N = 3$ independent HS lines: 10A, 21.31, and 21.35).

(B) In an independent experiment, the decreased ER Ca^{2+} levels in the LRRK2 neurons were confirmed ($p = 0.0425$, $F_{(2, 12)} = 4.155$, $N = 5$ [$N = 4$ independent PD patient lines with 1 line containing 2 clones]). LRRK2 ASO treatment of the LRRK2 neurons ($N = 5$ [$N = 4$ independent PD patient lines with 1 line containing 2 clones: 29F, 9A, PD28 clone 1 (C1), PD28 clone 2 (C2), and PD37]), inducing exon 41 skipping (ex41 ASO; see Figures S2B and S2C), rescues ER Ca^{2+} levels to match those observed in the HS iPSC-derived neurons ($N = 5$ independent HS lines: 10A, 21.31, 21.35, HS11A, and A6) treated with the Ctrl ASO ($p = 0.0425$, $F_{(2, 12)} = 4.155$) Only ASO-lissamine-positive cells were used for the analysis.

(C) Baseline ER Ca^{2+} levels are significantly lower in the iPSC-derived midbrain dopamine (DA) neurons carrying the LRRK2 G2019S mutation ($p < 0.0001$, Kruskal-Wallis statistic 57.32, $N = 1$ independent PD patient line: PD28 clone 2) compared with the HS controls ($N = 1$ independent HS line: 21.35). LRRK2 ex41 ASO (see Figure S2D) increased ER Ca^{2+} levels in LRRK2 DA neurons compared with the Ctrl ASO-treated cells ($p < 0.0001$, Kruskal-Wallis statistic 57.32). Data represent a pool of 3 technical replicates quantifying >150 neurons. Only ASO-lissamine-positive cells were used for the analysis.

(D and E) (D) ER Ca^{2+} efflux is not altered in the LRRK2 G2019S neurons ($N = 4$ [$N = 3$ independent PD patient lines with 1 line containing 2 clones: 29F, 9A, PD28 clone 1 (C1), and PD28 clone 2 (C2)]) compared with the HS controls ($N = 3$ independent HS lines: 10A, 21.31, and 21.35) upon KCl-stimulated ER Ca^{2+} release (green bar) at baseline, nor (E) after Serca inhibition induced by 24 hr treatment with 10 nM THP. The absolute GFP intensity in each line was normalized to the total intensity of that same line to correct for the virus infection rate. In

(legend continued on next page)

Table 1. Decreased mRNA Expression of Key ER Ca^{2+} Regulators and CamK1D in LRRK2 G2019S Neurons

	LRRK2 Gene Corrected	LRRK2 G2019S	t Test p Value
STIM1	1.84 ± 0.09	1.00 ± 0.17	0.005[a]
TRPC1	1.82 ± 0.16	1.09 ± 0.17	0.0209[b]
ORAI1	1.23 ± 0.03	0.94 ± 0.05	0.0038[a]
CAMK1D	2.1 ± 0.37	0.65 ± 0.21	0.015[b]
SERCA2	1.01 ± 0.08	0.71 ± 0.12	0.0875
SERCA3	0.77 ± 0.15	0.61 ± 0.29	0.6254
ITPR1	1.21 ± 0.15	0.77 ± 0.46	0.3937
ITPR3	1.70 ± 0.50	0.85 ± 0.30	0.1955
RyR2	1.60 ± 0.53	0.41 ± 0.11	0.0689
RyR3	1.39 ± 0.46	0.25 ± 0.16	0.0574

Gene expression changes in the key ER Ca^{2+} regulators and a previously found LRRK2 candidate interactor Ca^{2+}/calmodulin-dependent protein kinase type 1D (*CamK1D*; Beilina et al., 2014) in iPSC-derived neurons carrying the LRRK2 G2019S mutation (N = 4 [N = 2 independent PD patient lines with 2 clones per line: IM1Mut-L2-1Mut, IM2Mut-L2-2Mut, T4.6(Mut)-L1-1Mut, T4.13(Mut)-L1-2Mut]), relative to their isogenic GC controls (N = 4 [N = 2 independent GC lines with 2 clones per line: IM1GC-L2-1GC, IM2GC-L2-2GC, T4.6.43(GC)-L1-1GC2, T4.13.10(GC)-L1-2GC]). Values represent average gene expression levels of 4 iPSC lines per genotype, each line represented by a pool of 3 technical replicates, corrected for primer efficiency and *GAPDH* expression. SEM was calculated between the different iPSC lines.

[a]Statistical analysis was performed using two-tailed unpaired Student's t test, $p < 0.01$.

[b]Statistical analysis was performed using two-tailed unpaired Student's t test, $p < 0.05$.

DISCUSSION

The current findings show that inhibition of ER Ca^{2+} influx by THP induces neurite collapse in iPSC-derived PD patient neurons carrying the LRRK2 G2019S mutation, concurrent with higher extracellular Ca^{2+} uptake and a decreased intracellular Ca^{2+} buffering capacity in response to prolonged membrane depolarization. Furthermore, compartmentalized live-cell Ca^{2+} imaging demonstrated that the PD-associated LRRK2 G2019S mutation decreases ER Ca^{2+} levels. Finally, expression changes were seen in genes with key roles in ER-mediated Ca^{2+} entry in neurons with the LRRK2 G2019S mutation. Together these results point to an involvement of LRRK2 kinase in calcium homeostasis via regulation of ER Ca^{2+} levels, and a direct phenotypic cellular effect on axonal growth and integrity.

ER Calcium Control and Its Role in Neurodegenerative Disease

ER calcium store-operated impairments were identified in idiopathic and familial PD patient fibroblasts carrying the *PARK14* (Pla2g6) R747W mutation (Zhou et al., 2016). Typically, when ER Ca^{2+} stores are depleted, SOCE is initiated, activating the ER Ca^{2+} sensor STIM1 to open plasma membrane Ca^{2+} channels such as Ora1 and TRPC1 (Ambudkar et al., 2017). Alterations in ER Ca^{2+} release and lysosomal Ca^{2+} content are also observed in PD patient fibroblasts carrying *GBA1* mutations (Kilpatrick et al., 2016), and human *GBA1* iPSC-derived midbrain DA neurons show increased total Ca^{2+} and vulnerability to ER Ca^{2+} ionophore A23187 (Schondorf et al., 2014). Intriguingly, human brain tissue samples from Gaucher's disease (GD) type 2 patients, carrying homozygous *GBA1* mutations and characterized by neurological involvement, show enhanced Ca^{2+} release via RyRs (Pelled et al., 2005). Treatment of GD mice with the RyR antagonist dantrolene improved behavior and survival of these animals (Liou et al., 2016). *In vivo* mouse models of two other lipid storage disorders, Sandhoff disease and Niemann-Pick A disease, are both characterized by neurodegenerative phenotypes and show decreases in Serca activity (Pelled et al., 2003) or both Serca and inositol trisphosphate receptor 3 (IP3R) expression levels (Ginzburg and Futerman, 2005). Our findings of the LRRK2 G2019S mutation in human neurons producing decreased ER Ca^{2+} levels and increased neurite collapse after Serca inhibition further point to the importance of this system in neuronal vulnerability.

Neuronal Vulnerability and Calcium Control

Previous work has shown that the LRRK2 G2019S mutation increases cellular vulnerability in human PD patient fibroblasts (Smith et al., 2016) and iPSC-derived neurons (Cooper et al., 2012) when exposed to mitochondrial stressors. We now find that the LRRK2 G2019S mutation, known to induce an increase in LRRK2 kinase activity (Islam and Moore, 2017; West et al., 2005), plays a role in axonal vulnerability and modifies ER calcium control, potentially contributing to PD pathology (see schematic Figure 5).

The LRRK2 G2019S mutation influences axonal integrity (Reinhardt et al., 2013; Sanchez-Danes et al., 2012; Winner

(D) and (E) CEPIA-ER GFP levels were additionally normalized to the resting state (15–55 s) of each cell to detect the individual changes in ER Ca^{2+} levels upon Ca^{2+} efflux (ΔF). In each experiment, each line represents a pool of 3 technical replicates.

Statistical analysis was performed using Student's two-tailed t test, one-way ANOVA with Holm-Sidak MTC, or Kruskal-Wallis test with Dunn's MTC. *$p < 0.05$, ****$p < 0.0001$. In (C) outliers were identified using the ROUT method with 1% default Q value. Error bars represent SEM. See also Figures S2–S4.

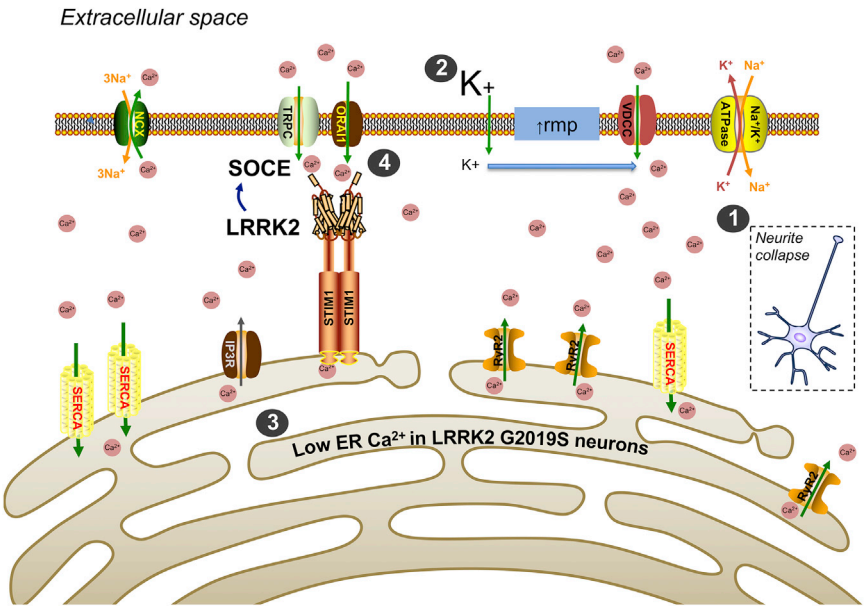

Figure 5. Hypothesized Role of LRRK2 in Intracellular and ER Calcium Homeostasis as Studied in Human iPSC-Derived Neurons

IPSC neurons carrying the LRRK2 G2019S mutation show increased neurite collapse upon SERCA inhibition (**1**, see Figure 2), altered Ca^{2+} uptake and intracellular Ca^{2+} buffering upon Serca inhibition and KCl depolarization (**2**, see Figure 3), decreased ER Ca^{2+} levels (**3**, see Figure 4), and decreased mRNA expression of key store-operated Ca^{2+} entry (SOCE) regulators (**4**, *STIM1*, *ORAI1*, *TRPC1*, see Table 1). Based on these data we hypothesize that LRRK2 plays a role in ER Ca^{2+} control, and the G2019S mutation, reported previously to increase the LRRK2 kinase activity (Islam and Moore, 2017; West et al., 2005), alters calcium homeostasis (Figures 3 and 4), consequently predisposing neurons carrying this mutation to an increased vulnerability of additional external ER stressors, observed here through an increased neurite collapse upon Serca inhibition (Figure 2). Legend: NCX, sodium Ca^{2+} exchanger (removes Ca^{2+} from the cell); TRPC, transient receptor potential cation channel, plays a role in SOCE Ca^{2+} entry; ORAI1, structural component of the Ca^{2+} release-activated channel, plays a role in SOCE Ca^{2+} entry; STIM1, stromal interaction molecule 1, ER Ca^{2+} sensor, plays a role in SOCE Ca^{2+} entry; rmp, resting membrane potential; VDCC, voltage-dependent Ca^{2+} channels, including L-type (cav1.1–1.4), N-type (cav2.2), and P/Q-type (cav2.1) channels; Na/K ATPase, sodium-potassium pump; IP3R, inositol 1,4,5-trisphosphate receptor, plays a role in SOCE Ca^{2+} entry; SERCA, sarco/ER Ca^{2+}-ATPase, ER Ca^{2+} pump; RyR, ryanodine receptor, intracellular Ca^{2+} channels, mediate Ca^{2+}-induced Ca^{2+} release.

et al., 2011) in a kinase activity-dependent manner (Sheng et al., 2012), with the current data presenting a specific kinase LRRK2 G2019S-dependent neurite collapse upon THP-induced SERCA inhibition, indicating a prominence of axonal vulnerability to alterations in ER Ca^{2+} levels. Indeed, these human iPSC-derived neurons show decreased ER Ca^{2+} levels already at baseline, possibly explained by reduced functionality of SOCE as a consequence of the decreased SOCE-related gene expression levels of *STIM1*, *TRPC1*, and *ORA1*. Corroborating this hypothesis, no changes were observed in the kinetics of CICR and ER Ca^{2+} efflux receptor expression.

An impact of ER Ca^{2+} levels on neurite outgrowth was seen in a hereditary model of spastic paraplegia induced by atlastin mutations, a neurodegenerative disorder characterized by a progressive gait disorder. In PC-12 cells, atlastin mutations inhibit nerve growth factor-stimulated neurite outgrowth by altering ER morphology and SOCE function through decreased STIM1 and ORA1 activation upon ER Ca^{2+} depletion (Li et al., 2017). Ca^{2+} release from intra-axonal ER Ca^{2+} stores contributes to secondary degradation of axons after spinal cord injury (Stirling et al., 2014). The current findings of reduced *TRPC1* expression in human LRRK2 G2019S neurons are interesting in this context, as surface membrane expression of TRPC1, a Ca^{2+} channel activated upon SOCE initiation, is essential for neurite outgrowth and axon guidance *in vitro* (Heo et al., 2012; Kerstein et al., 2013). Furthermore, inhibition of Cav1.3 channels through TRPC1-STIM1 complex influences DA neuron survival (Sun et al., 2017). Compromised ER calcium control in LRRK2 G2019S neurons could contribute to increased neuronal vulnerability. Indeed, after Serca inhibition, there was an extensive neurite collapse, increased Ca^{2+} uptake, and decreased intracellular Ca^{2+} buffering, indicating cellular dysfunction as a consequence of the alterations in ER Ca^{2+} regulation (Figure 5).

Changes in ER Ca^{2+} Levels May Influence Cell Organelle Function

ER Ca^{2+} levels and ER Ca^{2+} trafficking can affect ER function such as ER chaperone protein folding capacity, ER stress response, ER-driven lipid synthesis, ER stress-induced autophagy, transcription regulation, and calcium-induced cell death (Jacquemyn et al., 2017; Sano and Reed, 2013). The observed alterations in ER Ca^{2+} levels by the LRRK2 G2019S mutation can therefore have a dramatic effect on cell function. Since ER Ca^{2+} levels were rescued by a LRRK2-specific ASO, which decreases total LRRK2 protein levels, it is possible that other known LRRK2 mutations could also have an impact on ER calcium control. LRRK2

protein colocalizes with the ER in the human brain (Vitte et al., 2010) and is linked with the regulation of a major ER quality control protein chaperone, BiP (Yuan et al., 2011), suggesting a functional link between the ER and LRRK2.

The ER network extends throughout the cell, including the most distal structures, such as axons and dendrites in neurons. Apart from the ER membrane being connected to membranes of the secretory and endocytic pathway via vesicular pathways, ER is functionally connected to multiple organelles such as mitochondria, lysosomes, plasma membrane, multivesicular bodies, and endocytic vesicles via direct ER membrane contact sites (MCSs), sites for intracellular Ca^{2+} flux and lipid exchange (Saheki and De Camilli, 2017; Wu et al., 2017). ER Ca^{2+} can be translocated to lysosomes and mitochondria, regulating organelle communication and function (Lam and Galione, 2013). Changes in ER Ca^{2+} levels in LRRK2 G2019S human neurons may therefore contribute to alterations in Ca^{2+} transfer within the cell. ER-mitochondria MCSs are responsible for Ca^{2+} delivery into the inner mitochondrial membrane through IP3R and RyR ER Ca^{2+} channels and VDAC and MCU mitochondrial Ca^{2+} channels, influencing ATP production (reviewed in Krols et al., 2016; Lam and Galione, 2013). Mitochondria also play a significant role in intracellular Ca^{2+} store (Lam and Galione, 2013). In a broader perspective, an interplay between ER, mitochondria, and lysosome Ca^{2+} exchange may contribute to disease vulnerability since alterations in mitochondrial Ca^{2+} fluctuations and lysosomal Ca^{2+} impairments have been shown in models of familial and genetically linked PD (LRRK2, GBA, DJ1; Cherra et al., 2013; Gomez-Suaga et al., 2012; Guzman et al., 2010; Kilpatrick et al., 2016; Verma et al., 2017). These results point to an involvement of ER calcium control in the pathogenesis of PD, which is supported by our current findings on LRRK2 function and earlier findings of PARK14 (Zhou et al., 2016) and GBA1 (Kilpatrick et al., 2016; Schondorf et al., 2014) involvement in ER Ca^{2+} signaling.

ER receptor IP3R- and RyR-induced calcium release has been shown to be related to synaptic strength (Chakroborty et al., 2012; Deller et al., 2003). In the context of PD and calcium homeostasis in DA neuron function, this could be important as intracellular Ca^{2+} binding to the α-synuclein C terminus influences the strength of α-synuclein lipid membrane binding capacity, thereby modulating synaptic vesicle interactions (Lautenschlager et al., 2018). Such lipid-vesicle deposition of α-synuclein and p-Tau was recently shown to be altered in aging, the largest risk factor in PD (Brekk et al., 2018). LRRK2 G2019S-dependent changes in ER calcium control may therefore directly influence α-synuclein synaptic vesicle interaction and docking, a major role of α-synuclein in neuronal synaptic terminals (Logan et al., 2017). In conclusion, the LRRK2-dependent interactions with ER-dependent calcium homeostasis could be critical for PD pathogenesis.

EXPERIMENTAL PROCEDURES

iPSC Culture and Neuronal Differentiation

iPSCs were generated from PD patients carrying the LRRK2 G20919S mutation and HS controls (Cooper et al., 2012; Reinhardt et al., 2013) or were gene corrected using zinc finger nuclease technology as described in Reinhardt et al. (2013) (Table S1).

To obtain a broad range of human neuronal populations we differentiated iPSCs using a 35 day neuron differentiation protocol modified from Brennand et al. (2011), generating a mixture of glutamatergic, GABAergic, and dopaminergic neuronal subtypes. Midbrain DA neurons were differentiated using a protocol adapted from Cooper et al. (2010) and Sundberg et al. (2013) and shortened to 28 days.

LRRK2-Specific Antisense Oligomer Treatment, LRRK2 Exon Skipping Analysis, and LRRK2 Protein Expression Analysis

To demonstrate the specific LRRK2 G2019S mutation effect on our cellular phenotypes, a LRRK2 exon 41 antisense phosphorodiamidate morpholino oligomer (ex41 ASO) sequence was developed: 5′-AGACAGACCTGATCACCTACCTGGT-3′, binding to the pre-mRNA exon 41 sequence and inducing exon 41 skipping. As a control, a non-target standard control sequence (Ctrl ASO) was used: 5′-CCTCTTACCTCAGTTACAATTTATA-3′ (Gene Tools). In addition, ASOs with a carboxyfluorescein or lissamine tag emitting either green or red fluorescence (524.5 or 593.0 nm, respectively) were used to identify ASO-transduced positive cells. Exon skipping analysis was performed as described in Hinrich et al. (2016). Immunohistochemistry and western blot analysis for LRRK2 human protein detection (UDD3, MRC, University of Dundee) was performed on ASO-transfected iPSC-derived neurons 7 days post plating.

Neurite Outgrowth

Live-cell imaging, using the IncuCyte ZOOM live imaging system (Essen BioScience), was started immediately after plating in 96 well plate format. Seven days post plating, neurons were exposed to THP (Sigma T9033) at 0, 1, 10, and 100 nM concentrations. Neurite length per cell body cluster was measured using the Essen BioScience neurite analysis tool.

To evaluate ex41 ASO-induced rescue on neurite length, the IncuCyte ZOOM images of only ASO-carboxyfluorescein-positive neurons were manually traced in Fiji using the ImageJ NeuronJ plugin. Total neurite length was corrected for the number of ASO+ neurons.

Total Intracellular Live-Cell Ca^{2+} Imaging

ASO-transfected iPSC neurons were treated with either vehicle (EtOH) or 10 nM THP 7 days post plating. On day 8, total intracellular Ca^{2+} fura-2 AM (Molecular Probes, F1221) neuronal imaging was performed in standard external solution (SES) at emission

wavelengths of 340 and 380 nm, with an exposure time of 600 and 300 ms, respectively. To measure Ca^{2+} uptake, membrane depolarization was elicited with 50 mM KCl in SES for 15 s at 1 min and for 6 min at 5 min, every time followed by an SES wash. To identify ASO-carboxyfluorescein-positive cells, one image at 525 nm was acquired. For analysis, regions of interest (ROIs) were highlighted in ASO-carboxyfluorescein-positive cells and fura-2 AM 340 nm/380 nm fluorescence ratio was measured over time. The change in fluorescence was normalized to the baseline fluorescence prior to the first KCl stimulation (15–54 s). Only active cells with a minimum 7% fura-2 AM ratio change from baseline during the first KCl stimulation were included in the further analyses. Both the peak amplitudes of KCl-stimulated Ca^{2+} uptake and the area under the curve during the second KCl prolonged depolarization were analyzed, the latter representing the buffering of the unbound Ca^{2+} into compartmentalized organelle stores.

ER Ca^{2+} Live-Cell Imaging

To measure ER Ca^{2+} levels, a synapsin promotor-driven Ca^{2+}-measuring organelle-entrapped GFP ER indicator (CEPIA-ER GFP; Suzuki et al., 2014) was delivered to ASO-lissamine tag-transfected iPSC-derived neurons using a lentivirus. At day 8 post plating, neurons were imaged at 525 nm in SES for 1 min, followed by 15 s 50 mM KCl treatment and a 1 min wash with SES. Fiji ImageJ software with a Time Series Analyzer v.3 plugin was used to measure GFP levels in each ROI. ASO-lissamine tag-positive, GFP bleached-corrected, and lentivirus transduction efficiency-corrected cells, with a minimum of 2% decrease in GFP levels during KCl stimulation from their own baseline, were included in further analyses. Baseline ER Ca^{2+} levels were measured by averaging CEPIA-ER GFP intensity of each line in the first 15–55 s of imaging, prior to the KCl depolarization. ER CICR was measured by correcting the CEPIA-ER GFP fluorescence intensity at the maximum KCl-stimulated decrease to baseline levels, as described above.

qPCR Analysis of ER Ca^{2+} Regulators

RNA was isolated and purified according to the RNeasy spin column method (Qiagen, 74104) and cDNA was synthesized using the QuantiTect reverse transcription procedure (Qiagen, 205311). qPCR was run using the QuantiTect primer assays (Qiagen, Table S2), using a StepOnePlus real-time PCR system (Applied Biosystems) with a SybrGreen detection method (Applied Biosystems, 4367659). Sample cycle threshold values were normalized to the primer efficiency and to *GAPDH* housekeeping gene expression levels.

Statistical Analysis

Data analysis was performed in the GraphPad Prism software v.7.0c. All data are expressed as the mean ± SEM. Data were analyzed for normal distribution using the Shapiro-Wilk test and Normal Q-Q plot analysis in IBM SPSS software, v.20. Statistical analysis was performed using one-way ANOVA with Holm-Sidak multiple testing correction (MTC), Kruskal-Wallis with Dunn's MTC, repeated-measure one-way ANOVA with Dunnett's MTC, or Friedman test with Dunn's MTC when comparing between three groups or more. Unpaired Student's two-tailed t test or Mann-Whitney test was used when comparing between two genotype groups. Two-way ANOVA with Sidak's MTC was used when comparing the cellular genotype effect between different time points in culture. For each experiment, the test used is noted in the figure legend. A p value of <0.05 was considered significant for all analyses.

Detailed experimental procedures can be found in the Supplemental Experimental Procedures section.

SUPPLEMENTAL INFORMATION

Supplemental Information includes Supplemental Experimental Procedures, four figures, and two tables and can be found with this article online at https://doi.org/10.1016/j.stemcr.2018.11.021.

AUTHOR CONTRIBUTIONS

J.A.K., S.T., M.L.H., C.J.W., P.J.H., and O.I. contributed to the study design. J.A.K., S.T., T.O., S.M.L., S.L., E.J.F., A.M., E.A., F.M.J., and A.H. contributed to the experimental execution. J.A.K., S.T., S.M.L., S.L., M.L.H., C.J.W., P.J.H., and O.I. contributed to the data analysis and data review. J.A.K., S.T., P.J.H., and O.I. contributed to the manuscript generation.

ACKNOWLEDGMENTS

We would like to thank Dr. Sterneckert, Dr. Deleidi, Dr. Gasser, and Dr. Reinhardt for generously sharing a set of iPSCs from LRRK2 G2019S carrier PD patients and their gene-corrected isogenic controls (see Reinhardt et al., 2013), and the Boston Children's Hospital Viral Core for producing the CEPIA-ER-GFP lentivirus. The work reported here was supported by a grant from The Michael J. Fox Foundation (O.I.) and NIH grants 1RC2NS070276 and 1U24NS078338-01 awarded to the National Institute of Neurological Disorders and Stroke PD iPS Cell Research Consortium (O.I.). Additional support from The Consolidated Anti-Aging Foundation, The Orchard Foundation, The Cooper Family Fund for Parkinson's Research and The Poul Hansen Family (O.I.), National Institutes of Health grant R35NS105076 (C.J.W.), and the Canada Research Chair Award #950-231859 (S.T.) is also gratefully acknowledged.

Received: May 2, 2018
Revised: November 29, 2018
Accepted: November 30, 2018
Published: December 27, 2018

REFERENCES

Ambudkar, I.S., de Souza, L.B., and Ong, H.L. (2017). TRPC1, Orai1, and STIM1 in SOCE: friends in tight spaces. Cell Calcium *63*, 33–39.

Bedford, C., Sears, C., Perez-Carrion, M., Piccoli, G., and Condliffe, S.B. (2016). LRRK2 regulates voltage-gated calcium channel function. Front. Mol. Neurosci. *9*, 35.

Beilina, A., Rudenko, I.N., Kaganovich, A., Civiero, L., Chau, H., Kalia, S.K., Kalia, L.V., Lobbestael, E., Chia, R., Ndukwe, K., et al. (2014). Unbiased screen for interactors of leucine-rich repeat

kinase 2 supports a common pathway for sporadic and familial Parkinson disease. Proc. Natl. Acad. Sci. U S A *111*, 2626–2631.

Brekk, O.R., Moskites, A., Isacson, O., and Hallett, P.J. (2018). Lipid-dependent deposition of alpha-synuclein and Tau on neuronal Secretogranin II-positive vesicular membranes with age. Sci. Rep. *8*, 15207.

Brennand, K.J., Simone, A., Jou, J., Gelboin-Burkhart, C., Tran, N., Sangar, S., Li, Y., Mu, Y., Chen, G., Yu, D., et al. (2011). Modelling schizophrenia using human induced pluripotent stem cells. Nature *473*, 221–225.

Chakroborty, S., Kim, J., Schneider, C., Jacobson, C., Molgo, J., and Stutzmann, G.E. (2012). Early presynaptic and postsynaptic calcium signaling abnormalities mask underlying synaptic depression in presymptomatic Alzheimer's disease mice. J. Neurosci. *32*, 8341–8353.

Cherra, S.J., 3rd, Steer, E., Gusdon, A.M., Kiselyov, K., and Chu, C.T. (2013). Mutant LRRK2 elicits calcium imbalance and depletion of dendritic mitochondria in neurons. Am. J. Pathol. *182*, 474–484.

Cooper, O., Hargus, G., Deleidi, M., Blak, A., Osborn, T., Marlow, E., Lee, K., Levy, A., Perez-Torres, E., Yow, A., et al. (2010). Differentiation of human ES and Parkinson's disease iPS cells into ventral midbrain dopaminergic neurons requires a high activity form of SHH, FGF8a and specific regionalization by retinoic acid. Mol. Cell. Neurosci. *45*, 258–266.

Cooper, O., Seo, H., Andrabi, S., Guardia-Laguarta, C., Graziotto, J., Sundberg, M., McLean, J.R., Carrillo-Reid, L., Xie, Z., Osborn, T., et al. (2012). Pharmacological rescue of mitochondrial deficits in iPSC-derived neural cells from patients with familial Parkinson's disease. Sci. Transl. Med. *4*, 141ra190.

Deller, T., Korte, M., Chabanis, S., Drakew, A., Schwegler, H., Stefani, G.G., Zuniga, A., Schwarz, K., Bonhoeffer, T., Zeller, R., et al. (2003). Synaptopodin-deficient mice lack a spine apparatus and show deficits in synaptic plasticity. Proc. Natl. Acad. Sci. U S A *100*, 10494–10499.

Fell, M.J., Mirescu, C., Basu, K., Cheewatrakoolpong, B., DeMong, D.E., Ellis, J.M., Hyde, L.A., Lin, Y., Markgraf, C.G., Mei, H., et al. (2015). MLi-2, a potent, selective, and centrally active compound for exploring the therapeutic potential and safety of LRRK2 kinase inhibition. J. Pharmacol. Exp. Ther. *355*, 397–409.

Ginzburg, L., and Futerman, A.H. (2005). Defective calcium homeostasis in the cerebellum in a mouse model of Niemann-Pick A disease. J. Neurochem. *95*, 1619–1628.

Gomez-Suaga, P., Luzon-Toro, B., Churamani, D., Zhang, L., Bloor-Young, D., Patel, S., Woodman, P.G., Churchill, G.C., and Hilfiker, S. (2012). Leucine-rich repeat kinase 2 regulates autophagy through a calcium-dependent pathway involving NAADP. Hum. Mol. Genet. *21*, 511–525.

Guzman, J.N., Sanchez-Padilla, J., Wokosin, D., Kondapalli, J., Ilijic, E., Schumacker, P.T., and Surmeier, D.J. (2010). Oxidant stress evoked by pacemaking in dopaminergic neurons is attenuated by DJ-1. Nature *468*, 696–700.

Heo, D.K., Chung, W.Y., Park, H.W., Yuan, J.P., Lee, M.G., and Kim, J.Y. (2012). Opposite regulatory effects of TRPC1 and TRPC5 on neurite outgrowth in PC12 cells. Cell. Signal. *24*, 899–906.

Hinrich, A.J., Jodelka, F.M., Chang, J.L., Brutman, D., Bruno, A.M., Briggs, C.A., James, B.D., Stutzmann, G.E., Bennett, D.A., Miller, S.A., et al. (2016). Therapeutic correction of ApoER2 splicing in Alzheimer's disease mice using antisense oligonucleotides. EMBO Mol. Med. *8*, 328–345.

Hoozemans, J.J., van Haastert, E.S., Eikelenboom, P., de Vos, R.A., Rozemuller, J.M., and Scheper, W. (2007). Activation of the unfolded protein response in Parkinson's disease. Biochem. Biophys. Res. Commun. *354*, 707–711.

Hsieh, C.H., Shaltouki, A., Gonzalez, A.E., Bettencourt da Cruz, A., Burbulla, L.F., St Lawrence, E., Schule, B., Krainc, D., Palmer, T.D., and Wang, X. (2016). Functional impairment in Miro degradation and mitophagy is a shared feature in familial and sporadic Parkinson's disease. Cell Stem Cell *19*, 709–724.

Hurley, M.J., Brandon, B., Gentleman, S.M., and Dexter, D.T. (2013). Parkinson's disease is associated with altered expression of CaV1 channels and calcium-binding proteins. Brain *136*, 2077–2097.

Islam, M.S., and Moore, D.J. (2017). Mechanisms of LRRK2-dependent neurodegeneration: role of enzymatic activity and protein aggregation. Biochem. Soc. Trans. *45*, 163–172.

Jacquemyn, J., Cascalho, A., and Goodchild, R.E. (2017). The ins and outs of endoplasmic reticulum-controlled lipid biosynthesis. EMBO Rep. *18*, 1905–1921.

Kerstein, P.C., Jacques-Fricke, B.T., Rengifo, J., Mogen, B.J., Williams, J.C., Gottlieb, P.A., Sachs, F., and Gomez, T.M. (2013). Mechanosensitive TRPC1 channels promote calpain proteolysis of talin to regulate spinal axon outgrowth. J. Neurosci. *33*, 273–285.

Kilpatrick, B.S., Magalhaes, J., Beavan, M.S., McNeill, A., Gegg, M.E., Cleeter, M.W., Bloor-Young, D., Churchill, G.C., Duchen, M.R., Schapira, A.H., et al. (2016). Endoplasmic reticulum and lysosomal Ca(2)(+) stores are remodelled in GBA1-linked Parkinson disease patient fibroblasts. Cell Calcium *59*, 12–20.

Klemann, C., Martens, G.J.M., Sharma, M., Martens, M.B., Isacson, O., Gasser, T., Visser, J.E., and Poelmans, G. (2017). Integrated molecular landscape of Parkinson's disease. NPJ Parkinsons Dis. *3*, 14.

Krols, M., van Isterdael, G., Asselbergh, B., Kremer, A., Lippens, S., Timmerman, V., and Janssens, S. (2016). Mitochondria-associated membranes as hubs for neurodegeneration. Acta Neuropathol. *131*, 505–523.

Lam, A.K., and Galione, A. (2013). The endoplasmic reticulum and junctional membrane communication during calcium signaling. Biochim. Biophys. Acta *1833*, 2542–2559.

Lautenschlager, J., Stephens, A.D., Fusco, G., Strohl, F., Curry, N., Zacharopoulou, M., Michel, C.H., Laine, R., Nespovitaya, N., Fantham, M., et al. (2018). C-terminal calcium binding of alpha-synuclein modulates synaptic vesicle interaction. Nat. Commun. *9*, 712.

Li, J., Yan, B., Si, H., Peng, X., Zhang, S.L., and Hu, J. (2017). Atlastin regulates store-operated calcium entry for nerve growth factor-induced neurite outgrowth. Sci. Rep. *7*, 43490.

Liou, B., Peng, Y., Li, R., Inskeep, V., Zhang, W., Quinn, B., Dasgupta, N., Blackwood, R., Setchell, K.D., Fleming, S., et al. (2016). Modulating ryanodine receptors with dantrolene attenuates

neuronopathic phenotype in Gaucher disease mice. Hum. Mol. Genet. *25*, 5126–5141.

Logan, T., Bendor, J., Toupin, C., Thorn, K., and Edwards, R.H. (2017). alpha-Synuclein promotes dilation of the exocytotic fusion pore. Nat. Neurosci. *20*, 681–689.

Nalls, M.A., Pankratz, N., Lill, C.M., Do, C.B., Hernandez, D.G., Saad, M., DeStefano, A.L., Kara, E., Bras, J., Sharma, M., et al. (2014). Large-scale meta-analysis of genome-wide association data identifies six new risk loci for Parkinson's disease. Nat. Genet. *46*, 989–993.

Pelled, D., Lloyd-Evans, E., Riebeling, C., Jeyakumar, M., Platt, F.M., and Futerman, A.H. (2003). Inhibition of calcium uptake via the sarco/endoplasmic reticulum Ca^{2+}-ATPase in a mouse model of Sandhoff disease and prevention by treatment with N-butyldeoxynojirimycin. J. Biol. Chem. *278*, 29496–29501.

Pelled, D., Trajkovic-Bodennec, S., Lloyd-Evans, E., Sidransky, E., Schiffmann, R., and Futerman, A.H. (2005). Enhanced calcium release in the acute neuronopathic form of Gaucher disease. Neurobiol. Dis. *18*, 83–88.

Reinhardt, P., Schmid, B., Burbulla, L.F., Schondorf, D.C., Wagner, L., Glatza, M., Hoing, S., Hargus, G., Heck, S.A., Dhingra, A., et al. (2013). Genetic correction of a LRRK2 mutation in human iPSCs links parkinsonian neurodegeneration to ERK-dependent changes in gene expression. Cell Stem Cell *12*, 354–367.

Rivero-Rios, P., Gomez-Suaga, P., Fernandez, B., Madero-Perez, J., Schwab, A.J., Ebert, A.D., and Hilfiker, S. (2015). Alterations in late endocytic trafficking related to the pathobiology of LRRK2-linked Parkinson's disease. Biochem. Soc. Trans. *43*, 390–395.

Saheki, Y., and De Camilli, P. (2017). Endoplasmic reticulum-plasma membrane contact sites. Annu. Rev. Biochem. *86*, 659–684.

Sanchez-Danes, A., Richaud-Patin, Y., Carballo-Carbajal, I., Jimenez-Delgado, S., Caig, C., Mora, S., Di Guglielmo, C., Ezquerra, M., Patel, B., Giralt, A., et al. (2012). Disease-specific phenotypes in dopamine neurons from human iPS-based models of genetic and sporadic Parkinson's disease. EMBO Mol. Med. *4*, 380–395.

Sanders, L.H., Laganiere, J., Cooper, O., Mak, S.K., Vu, B.J., Huang, Y.A., Paschon, D.E., Vangipuram, M., Sundararajan, R., Urnov, F.D., et al. (2014). LRRK2 mutations cause mitochondrial DNA damage in iPSC-derived neural cells from Parkinson's disease patients: reversal by gene correction. Neurobiol. Dis. *62*, 381–386.

Sano, R., and Reed, J.C. (2013). ER stress-induced cell death mechanisms. Biochim. Biophys. Acta *1833*, 3460–3470.

Schapansky, J., Nardozzi, J.D., Felizia, F., and LaVoie, M.J. (2014). Membrane recruitment of endogenous LRRK2 precedes its potent regulation of autophagy. Hum. Mol. Genet. *23*, 4201–4214.

Schondorf, D.C., Aureli, M., McAllister, F.E., Hindley, C.J., Mayer, F., Schmid, B., Sardi, S.P., Valsecchi, M., Hoffmann, S., Schwarz, L.K., et al. (2014). iPSC-derived neurons from GBA1-associated Parkinson's disease patients show autophagic defects and impaired calcium homeostasis. Nat. Commun. *5*, 4028.

Schwab, A.J., and Ebert, A.D. (2015). Neurite aggregation and calcium dysfunction in iPSC-derived sensory neurons with Parkinson's disease-related LRRK2 G2019S mutation. Stem Cell Reports *5*, 1039–1052.

Sheng, Z., Zhang, S., Bustos, D., Kleinheinz, T., Le Pichon, C.E., Dominguez, S.L., Solanoy, H.O., Drummond, J., Zhang, X., Ding, X., et al. (2012). Ser1292 autophosphorylation is an indicator of LRRK2 kinase activity and contributes to the cellular effects of PD mutations. Sci. Transl. Med. *4*, 164ra161.

Smith, G.A., Jansson, J., Rocha, E.M., Osborn, T., Hallett, P.J., and Isacson, O. (2016). Fibroblast biomarkers of sporadic Parkinson's disease and LRRK2 kinase inhibition. Mol. Neurobiol. *53*, 5161–5177.

Steger, M., Tonelli, F., Ito, G., Davies, P., Trost, M., Vetter, M., Wachter, S., Lorentzen, E., Duddy, G., Wilson, S., et al. (2016). Phosphoproteomics reveals that Parkinson's disease kinase LRRK2 regulates a subset of Rab GTPases. Elife *5*, e12813.

Stirling, D.P., Cummins, K., Wayne Chen, S.R., and Stys, P. (2014). Axoplasmic reticulum Ca(2+) release causes secondary degeneration of spinal axons. Ann. Neurol. *75*, 220–229.

Sun, Y., Zhang, H., Selvaraj, S., Sukumaran, P., Lei, S., Birnbaumer, L., and Singh, B.B. (2017). Inhibition of L-type Ca(2+) channels by TRPC1-STIM1 complex is essential for the protection of dopaminergic neurons. J. Neurosci. *37*, 3364–3377.

Sundberg, M., Bogetofte, H., Lawson, T., Jansson, J., Smith, G., Astradsson, A., Moore, M., Osborn, T., Cooper, O., Spealman, R., et al. (2013). Improved cell therapy protocols for Parkinson's disease based on differentiation efficiency and safety of hESC-, hiPSC-, and non-human primate iPSC-derived dopaminergic neurons. Stem Cells *31*, 1548–1562.

Suzuki, J., Kanemaru, K., Ishii, K., Ohkura, M., Okubo, Y., and Iino, M. (2014). Imaging intraorganellar Ca^{2+} at subcellular resolution using CEPIA. Nat. Commun. *5*, 4153.

Verma, M., Callio, J., Otero, P.A., Sekler, I., Wills, Z.P., and Chu, C.T. (2017). Mitochondrial calcium dysregulation contributes to dendrite degeneration mediated by PD/LBD-associated LRRK2 mutants. J. Neurosci. *37*, 11151–11165.

Vitte, J., Traver, S., Maues De Paula, A., Lesage, S., Rovelli, G., Corti, O., Duyckaerts, C., and Brice, A. (2010). Leucine-rich repeat kinase 2 is associated with the endoplasmic reticulum in dopaminergic neurons and accumulates in the core of Lewy bodies in Parkinson disease. J. Neuropathol. Exp. Neurol. *69*, 959–972.

West, A.B., Moore, D.J., Biskup, S., Bugayenko, A., Smith, W.W., Ross, C.A., Dawson, V.L., and Dawson, T.M. (2005). Parkinson's disease-associated mutations in leucine-rich repeat kinase 2 augment kinase activity. Proc. Natl. Acad. Sci. U S A *102*, 16842–16847.

Winner, B., Melrose, H.L., Zhao, C., Hinkle, K.M., Yue, M., Kent, C., Braithwaite, A.T., Ogholikhan, S., Aigner, R., Winkler, J., et al. (2011). Adult neurogenesis and neurite outgrowth are impaired in LRRK2 G2019S mice. Neurobiol. Dis. *41*, 706–716.

Wu, K.D., Lee, W.S., Wey, J., Bungard, D., and Lytton, J. (1995). Localization and quantification of endoplasmic reticulum Ca(2+)-ATPase isoform transcripts. Am. J. Physiol. *269*, C775–C784.

Wu, Y., Whiteus, C., Xu, C.S., Hayworth, K.J., Weinberg, R.J., Hess, H.F., and De Camilli, P. (2017). Contacts between the endoplasmic reticulum and other membranes in neurons. Proc. Natl. Acad. Sci. U S A *114*, E4859–E4867.

Yan, J., Almilaji, A., Schmid, E., Elvira, B., Shimshek, D.R., van der Putten, H., Wagner, C.A., Shumilina, E., and Lang, F. (2015). Leucine-rich repeat kinase 2-sensitive Na^+/Ca^{2+} exchanger activity in dendritic cells. FASEB J. *29*, 1701–1710.

Yuan, Y., Cao, P., Smith, M.A., Kramp, K., Huang, Y., Hisamoto, N., Matsumoto, K., Hatzoglou, M., Jin, H., and Feng, Z. (2011). Dysregulated LRRK2 signaling in response to endoplasmic reticulum stress leads to dopaminergic neuron degeneration in C. elegans. PLoS One *6*, e22354.

Zhou, Q., Yen, A., Rymarczyk, G., Asai, H., Trengrove, C., Aziz, N., Kirber, M.T., Mostoslavsky, G., Ikezu, T., Wolozin, B., et al. (2016). Impairment of PARK14-dependent Ca(2+) signalling is a novel determinant of Parkinson's disease. Nat. Commun. *7*, 10332.